ResearchGate

See discussions, stats, and author profiles for this publication at: https://www.researchgate.net/publication/5919755

Developing Sensors for Real-Time Measurement of High Ca 2+ Concentrations †

ARTICLE *in* BIOCHEMISTRY · NOVEMBER 2007

Impact Factor: 3.02 · DOI: 10.1021/bi7007307 · Source: PubMed

CITATIONS
33

READS
36

13 AUTHORS, INCLUDING:

Aldebaran M Hofer
Brigham and Women's Hospital
43 PUBLICATIONS **1,993** CITATIONS
SEE PROFILE

Giovanni Gadda
Georgia State University
106 PUBLICATIONS **1,615** CITATIONS
SEE PROFILE

Angela Holder
Centers for Disease Control and Prevention
14 PUBLICATIONS **301** CITATIONS
SEE PROFILE

Kristy Welshhans
Kent State University
11 PUBLICATIONS **243** CITATIONS
SEE PROFILE

All in-text references underlined in blue are linked to publications on ResearchGate, letting you access and read them immediately.

Available from: Kristy Welshhans
Retrieved on: 26 January 2016

Developing Sensors for Real-Time Measurement of High Ca^{2+} Concentrations†

Jin Zou,‡ Aldebaran M. Hofer,§ Monica M. Lurtz,‖ Giovanni Gadda,‡ April L. Ellis,‡ Ning Chen,‡ Yun Huang,‡ Angela Holder,‡ Yiming Ye,‡ Charles F. Louis,‖ Kristy Welshhans,‡ Vincent Rehder,‡ and Jenny J. Yang*,‡

Departments of Chemistry and Biology, Center for Drug Design and Biotechnology, Georgia State University, Atlanta, Georgia 30303, Department of Surgery, Harvard Medical School, Brigham and Women's Hospital and VA Boston Healthcare System, West Roxbury, Massachusetts 02132, and Department of Cell Biology and Neuroscience, University of California, Riverside, California 92521

Received April 17, 2007; Revised Manuscript Received July 6, 2007

ABSTRACT: Ca^{2+} regulates numerous biological processes through spatiotemporal changes in the cytosolic Ca^{2+} concentration and subsequent interactions with Ca^{2+} binding proteins. The endoplasmic reticulum (ER) serves as an intracellular Ca^{2+} store and plays an essential role in cytosolic Ca^{2+} homeostasis. There is a strong need to develop Ca^{2+} sensors capable of real-time quantitative Ca^{2+} concentration measurements in specific subcellular environments without using natural Ca^{2+} binding proteins such as calmodulin, which themselves participate as signaling molecules in cells. In this report, a strategy for creating such sensors by grafting a Ca^{2+}-binding motif into chromophore sensitive locations in green fluorescence protein is described. The engineered Ca^{2+} sensors exhibit large ratiometric fluorescence and absorbance changes upon Ca^{2+} binding with affinities corresponding to the Ca^{2+} concentrations found in the ER (K_d values range from 0.4 to 2 mM). In addition to characterizing the optical and metal binding properties of the newly developed Ca^{2+} sensors with various spectroscopic methods, we also examined the kinetic properties using stopped-flow spectrofluorimetry to ensure accurate monitoring of dynamic Ca^{2+} changes. The developed Ca^{2+} sensor was successfully targeted to the ER of mammalian cell lines to monitor Ca^{2+} changes occurring in this compartment in response to stimulation with agonists. We envision that this class of Ca^{2+} sensors can be modified further to measure the Ca^{2+} concentration in other cellular compartments, providing tools for studying the contribution of these compartments to cellular Ca^{2+} signaling.

Ca^{2+} regulates many biological processes, including neuronal signaling, muscle contraction, cell development, and proliferation (*1*−*3*). Depending on their intracellular location, Ca^{2+} signals vary in amplitude and duration, together forming a complex Ca^{2+} signaling code. The endoplasmic reticulum (ER)[1] functions as the primary intracellular Ca^{2+} store (*4*−*7*) and is the site of protein synthesis and processing. Disruption of ER Ca^{2+} homeostasis triggers the ER stress response, a source of cell death signals (*8*, *9*). The release of Ca^{2+} from ER stores results in a rapid increase in $[Ca^{2+}]_c$, and the released Ca^{2+} binds to a number of intracellular Ca^{2+}-sensing proteins, such as calmodulin (CaM) and troponin C (TnC), as well as ion channels and enzymes to regulate a variety of cellular events and processes (*1*, *10*−*14*). Several human diseases, including various cardiomyopathies, Alzheimer's disease, cancer, and lens cataract formation, are known to be associated with altered Ca^{2+} signaling and altered Ca^{2+} regulation by the ER store (*1*, *3*, *13*, *15*−*17*).

Because of the essential role of the ER in Ca^{2+} signaling, the determination of free $[Ca^{2+}]_{ER}$ and its dynamic changes during cell signaling has attracted extensive interest. However, the lack of tractable biological Ca^{2+} indicators with affinities in the high micromolar to millimolar range has made it difficult to directly assess changes in $[Ca^{2+}]_{ER}$. Current estimates of $[Ca^{2+}]_{ER}$ have been derived using three major types of Ca^{2+} indicators and sensors (*18*−*23*). These are (1) synthetic small molecule fluorescent indicators such as Mag-Fura-2, (2) specifically modified derivatives of the chemiluminescent protein (photoprotein) aequorin, and (3) fluorescent indicators based on green fluorescence protein (GFP) variants with CaM or TnC. Although some small

† This work is supported in part by the following sponsors: NIH Grant GM070555 to J.J.Y. and C.F.L., GSU Brain and Behavior grant to J.J.Y. and V.R., NIH Grant GM62999 and NSF Grant MCB-0092486 to J.J.Y., NIH Grant EY-05684 to C.F.L., NSF Grant MCB-0545712, a VA Merit award to A.M.H., Career Award MCB-0545712 from NSF and PRF Grant 47636-AC4 to G.G., a GSU Brain and Behavior graduate fellowship to K.W., and AHA and GSU Brain and Behavior Predoctoral Fellowships to A.L.E.

* To whom correspondence should be addressed. Fax: (404) 413-5551. Telephone: (404) 413-5520. E-mail: chejjy@langate.gsu.edu.

‡ Georgia State University.

§ Brigham and Women's Hospital and VA Boston Healthcare System.

‖ University of California.

[1] Abbreviations: ADP, adenosine diphosphate; Amp, amplitude; ATP, adenosine triphosphate; CaM, calmodulin; CD, circular dichroism; CRsig, ER targeting sequence of calreticulin; DMEM, Dulbecco's modified Eagle's medium; ER, endoplasmic reticulum; FBS, fetal bovine serum; FPLC, fast performance liquid chromatography; FRET, fluorescence resonance energy transfer; GDP, guanosine diphosphate; GFP, green fluorescence protein; GSH, glutathione; GTP, guanosine triphosphate; IPTG, isopropyl β-D-thiogalactoside; HBSS, Hank's Balanced Salt Solution; Pen/Strep, penicillin and streptomycin; TnC, troponin C; UV−vis, ultraviolet and visible; YFP, yellow fluorescent protein.

10.1021/bi7007307 CCC: $37.00 © 2007 American Chemical Society
Published on Web 10/09/2007

molecule dyes accumulate in certain cellular compartments of cells, they cannot be unambiguously targeted to specific intracellular locations (*24*); invasive methods are frequently required to eliminate the large fluorescence background resulting from the presence of these dyes in the cytosol (*25*−*27*). Although the targeted aequorins overcome some of the problems associated with the compartmentalized dye approach, the low light output of these probes and the requirement for a soluble cofactor (coelenterazine) limit their usefulness (*28*).

GFP-based Ca^{2+} sensors, such as cameleons and pericams originally engineered by the groups of Miyawaki, Persechini, and Tsien, are based on either fluorescence resonance energy transfer (FRET) between two different GFP variants or the effect of a Ca^{2+}-dependent conformational change in natural Ca^{2+}-sensing proteins (e.g., CaM) on the protonation state of the chromophore of a single GFP variant (*29*−*35*). Because these sensors are based on naturally occurring essential Ca^{2+} binding proteins, a perturbation of the cellular environment through their introduction cannot be excluded, although many efforts have been made to minimize this possibility (*32*, *34*, *36*−*38*). Thus, there is a need to develop Ca^{2+} sensors that minimally compete for Ca^{2+} with existing cellular Ca^{2+} binding proteins and/or its target proteins, show robust Ca^{2+} responses, and exhibit Ca^{2+} binding affinities comparable to that of different cellular compartments, such as the ER.

In this report, we describe a new strategy for creating Ca^{2+} sensors by engineering a Ca^{2+}-binding motif into sensitive locations of a fluorescent protein without the use of FRET pairs. A series of Ca^{2+} sensors exhibiting large ratiometric fluorescence and absorbance changes upon Ca^{2+} binding was developed that have Ca^{2+} binding affinities corresponding to the $[Ca^{2+}]_{ER}$ (K_d values range from 0.4 to 2 mM). In addition to the detailed characterization of the optical and metal binding properties of the newly developed Ca^{2+} sensors with various spectroscopic methods, including visible absorption spectroscopy, circular dichroism (CD), and fluorescence spectroscopy, we have also examined their kinetic properties, which are important for the accurate monitoring of the dynamic properties of Ca^{2+} in living cells. The developed Ca^{2+} sensors have been successfully targeted to the ER in a mammalian cell line (BHK-21) to monitor changes in $[Ca^{2+}]_{ER}$ in response to stimulation with agonists. Future modifications to these sensors will render them potentially important tools in the study of Ca^{2+} dynamics in other cellular compartments.

MATERIALS AND METHODS

Construction of EGFP-Based Ca^{2+} Sensors. The Ca^{2+} binding motifs of CaM, loop III (DKDGNGYISAAE) and EF-hand motif (EEEIREAFRVFDKDGNGYISAAELRHVMTNL), were inserted into enhanced GFP (EGFP) as previously reported (*39*), and the insertions were verified by automated DNA sequencing. In brief, the cDNA encoding the EGFP variant grafted with a Ca^{2+} binding motif was cloned into bacterial and mammalian expression vectors between BamHI and EcoRI restriction enzyme sites. For bacterial expression, the pET28(a) vector with a six-His tag was utilized. For mammalian expression, the protein-encoding DNA was subcloned into a pcDNA3.1+ vector. The ER retention sequence, KDEL, was attached to the C-terminus, and the ER targeting sequence of calreticulin (CRsig), MLLSVPLLLGLLGLAAAD, was attached to the N-terminus of the EGFP-based Ca^{2+} sensors via PCR (*39*). The Kozak consensus sequence was placed at the N-terminus of the calreticulin sequence for the optimal initiation of protein expression in mammalian cells (*31*, *40*). DsRed2-ER (BD Biosciences Clontech), which contains CRsig and KDEL signal peptides at the N- and C-termini, respectively, was used as a marker for the ER in colocalization experiments. To improve the folding at 37 °C, two additional mutations, M153T and V163A, were also added to the Ca^{2+} sensors (*41*, *42*).

Expression and Purification of EGFP and Its Variants. EGFP and its variants were expressed in *Escherichia coli* BL21(DE3). Cells were grown at 37 °C in LB medium containing 30 μg/mL kanamycin to an OD_{600} of >0.6 before protein induction with 0.2 mM isopropyl β-D-thiogalactoside (IPTG). Since EGFP exhibits reduced fluorescence at 37 °C in vivo, high-level expression of the soluble mature form of EGFP was achieved by growing the cultures overnight in LB broth at 30 °C. EGFP and its variants were purified by sonication of the cell pellet and centrifugation at 22500*g* for 20 min. The supernatant was injected into a fast performance liquid chromatography (FPLC) system, AKTAprime, connected to a Hitrap Ni^{2+} chelating column (Amersham Biosciences). The protein was eluted from the column with a gradient of imidazole in 50 mM NaH_2PO_4/Na_2HPO_4 and 250 mM NaCl (pH 7.4) and identified by mass spectrometry. Imidazole was removed by dialysis against 10 mM Tris and 1 mM DTT (pH 7.4).

Ultraviolet and Visible Absorption Spectroscopy. Ultraviolet and visible (UV−vis) absorption spectra of EGFP and its variants were determined with a Shimadzu UV-1601 spectrophotometer. Protein concentrations were determined by UV−vis absorbance at 280 nm using a molar extinction coefficient of 21 890 M^{-1} cm^{-1} for EGFP-wt calculated from the contribution from aromatic residues (one Trp and 11 Tyr residues) (5500 and 1490 M^{-1} cm^{-1} for Trp and Tyr, respectively). The extinction coefficients (at 398 or 490 nm) of the EGFP variants were obtained with eq 1:

$$\epsilon_p = \epsilon_{p,280nm}\left(\frac{A_p}{A_{p,280nm}}\right) \quad (1)$$

where ϵ_p is the extinction coefficient at 398 or 490 nm of EGFP variants, $\epsilon_{p,280nm}$ is the extinction coefficient at 280 nm of EGFP variants, A_p is the absorption of EGFP variants at 398 or 490 nm, and $A_{p,280nm}$ is the absorption of EGFP variants at 280 nm. EGFP was used as a reference in the measurement of the extinction coefficients of the EGFP variants.

Fluorescence Spectroscopy. The properties of EGFP and its variants were monitored using a fluorescence spectrophotometer (Photon Technology International, Inc.) with a 10 mm path length quartz cell at 20 °C. Fluorescence spectra of the chromophore in proteins were measured in the emission region of 410−600 and 500−600 nm with 398 and 490 nm excitation wavelengths, respectively. The ratio of emissions in the range 500−600 nm when excited at 398 and 490 nm as a function of Ca^{2+} concentrations was utilized to calculate the apparent dissociation constant K_d for binding

of Ca^{2+} of various EGFP-based Ca^{2+} sensors by fitting eq 2 with a 1:1 metal binding equation:

$$f = \frac{[P]_T + [Ca]_T + K_d - \sqrt{([P]_T + [Ca]_T + K_d)^2 - 4[P]_T[Ca]_T}}{2[P]_T} \quad (2)$$

where f is the fraction of Ca^{2+}-bound protein, $[P]_T$ is the total protein concentration (millimolar), $[Ca]_T$ is the total Ca^{2+} concentration (millimolar), and K_d is the protein's apparent dissociation constant for Ca^{2+} binding. The fraction of the protein bound with Ca^{2+} was calculated according to eq 3:

$$f = \frac{R - R_{min}}{R_{max} - R_{min}} \quad (3)$$

where R_{min}, R, and R_{max} are the fluorescence emission ratios (excited at 398 and 490 nm) or the amplitudes measured with a stopped-flow spectrofluorimeter for Ca^{2+}-free, Ca^{2+}-bound, and Ca^{2+}-saturated protein, respectively. The fluorescence emission ratio (excited at 398 and 490 nm) was obtained by fitting the data to eq 4:

$$R = \frac{F_{(398nm)}}{F_{(490nm)}} \quad (4)$$

where $F_{(398nm)}$ and $F_{(490nm)}$ are the integrated fluorescence intensities in the range of 500−600 nm excited at 398 and 490 nm, respectively. The dynamic range value of Ca^{2+} sensors was calculated by dividing the fluorescence emission ratio excited at 398 and 490 nm of the Ca^{2+}-saturated state (R_{max}) with that of the Ca^{2+}-free state (R_{min}).

The apparent dissociation constant for Ca^{2+} binding (K_d) of EGFP-based Ca^{2+} sensors was also measured by competitive titration with rhodamine-5N. Rhodamine-5N is a fluorescent dye (Molecular Probes) (*43*) with a K_d of 319 ± 13 μM for Ca^{2+} in 100 mM Tris (pH 7.4). The dye concentration was calculated using an extinction coefficient of 63 000 M^{-1} cm^{-1} at 552 nm. Measurements with different Ca^{2+} concentrations were performed by maintaining the concentration of dye (10 μM) and protein constant. The fluorescence emission signal from 560 to 650 nm was measured with a cuvette with a path length of 10 mm excited at 552 nm. The slit widths of excitation and emission were set at 2 and 4 nm, respectively. The apparent dissociation constants were obtained by globally fitting the spectra from 560 to 650 nm using Specfit/32 with the metal and two-ligand model (Spectrum Software Associates) (*44*).

The Ca^{2+} selectivity of the EGFP-based Ca^{2+} sensor was examined by monitoring the change in the fluorescence ratio $F_{(398nm)}/F_{(490nm)}$ with 1.0 mM Ca^{2+} in the presence of metal ions, including 0.1 μM Cu^{2+}, 0.1 mM Zn^{2+}, 10.0 mM Mg^{2+}, 5.0 μM Tb^{3+}, or 5.0 μM La^{3+}. The normalized change in the ratio (ΔR) was calculated using eq 5:

$$\Delta R = \frac{R_{metal} - R_0}{R_{Ca} - R_0} \times 100 \quad (5)$$

where R_0 is the ratio of the EGFP-based Ca^{2+} sensor in the absence of Ca^{2+} and metal ions, R_{Ca} is the ratio of the EGFP-based Ca^{2+} sensor with 1.0 mM Ca^{2+} in the absence of metal ions, and R_{metal} is the ratio of the EGFP-based Ca^{2+} sensor with 1.0 mM Ca^{2+} in the presence of the metal ions. Equation 5 was also used to examine the effect of small molecules, including adenosine triphosphate (ATP), adenosine diphosphate (ADP), guanosine triphosphate (GTP), guanosine diphosphate (GDP), and glutathione (GSH) on the Ca^{2+} response of GFP-based Ca^{2+} sensors. Data are expressed as a percentage.

Stopped-Flow Spectrofluorimetry. Stopped-flow kinetic measurements were performed on a Hi-Tech SF-61 stopped-flow spectrofluorimeter (10 mm path length, dead time of <2 ms) with a 1:1 (v/v) ratio of the protein sensor and calcium at 20 °C, as described previously (*45*). Fluorescence emission changes associated with binding of Ca^{2+} to Ca-G1 were determined by mixing Ca^{2+} and Ca-G1 in 10 mM Tris and 1 mM DTT (pH 7.4) with excitation at 398 nm and a long-pass 455 nm filter. The concentrations of Ca^{2+} ranged from 0 to 10 mM. Fluorescence emission changes associated with dissociation of Ca^{2+} from Ca-G1 were measured upon mixing Ca-G1 preloaded with Ca^{2+} in 10 mM Tris and 1 mM DTT (pH 7.4) with the same buffer. Generally, six duplicate measurements were carried out for each point, and the last three were fitted to obtain the observed rate, k_{obs}. The k_{obs} for each Ca^{2+} concentration was obtained by fitting of the stopped-flow traces according to the single-exponential function shown in eq 6:

$$F_t = F_0 + Amp[1 - \exp(-k_{obs}t)] \quad (6)$$

where F_t is the fluorescence intensity at any stopped-flow time, F_0 is the initial fluorescence intensity, Amp is the final value of the fluorescence signal at the end of the process at a given Ca^{2+} concentration, k_{obs} is the observed rate of fluorescence change (s^{-1}), and t is the reaction time (s). Measurements typically differed by less than 1% between duplicate experiments.

Cell Culture and Transfection. Both BHK-21 and HeLa cells were grown on 100 mm culture dishes or glass coverslips (0.5−1.0 × 10^6 cells/dish) in 35 mm culture dishes in Dulbecco's modified Eagle's medium (DMEM, Sigma Chemical Co., St. Louis, MO) with 44 mM $NaHCO_3$ (pH 7.2) and supplemented with 10% (v/v) fetal bovine serum (FBS), 100 units/mL penicillin, and 0.1 mg/mL streptomycin (Pen/Strep) at 37 °C with 5% CO_2 in a humidified incubation chamber. The cells were seeded and grown overnight before transient transfection with Ca^{2+} sensor plasmid constructs.

Plasmid DNA used for transfection was harvested from transformed *E. coli* (DH5α) using a QIAGEN Miniprep protocol (Qiagen). Each of the EGFP variants was individually and transiently transfected into BHK-21 and HeLa cells with Lipofectamine-2000 (Invitrogen Life Technologies) and serum-free Opti-MEMI (Gibco Invitrogen Corp.) per the manufacturer's instructions. The plasmid DNA (2 μg) with a ratio of DNA to Lipofectamine between 1:1 and 1:3 (micrograms per microliter) was generally used in a typical transfection. Following incubation at 37 °C for 4 h, the medium containing the DNA−Lipofectamine complex was removed and replaced with DMEM enriched with FBS and Pen/Strep. The cells were then grown for 1−3 days in a humidified chamber with 5% CO_2 at 30 or 37 °C before fluorescence or confocal microscope imaging.

Confocal Microscope Imaging. BHK-21 and HeLa cells were transferred from DMEM to Hank's Balanced Salt Solution without divalent cations [HBSS(−), Sigma Chemi-

cal Co.] and media with 10 mM HEPES, 5 mM $NaHCO_3$, and 1 mM EGTA (pH 7.2) for live imaging experiments on an LSM 510 laser confocal microscope (Carl Zeiss Inc., Thornwood, NY) using a 100× oil-immersion objective (Zeiss, Fluar, 1.30 n.a.). Prior to imaging, cells and buffers were brought to ambient temperature and allowed to equilibrate to room air. The localization of EGFP-based Ca^{2+} sensors was visualized by excitation of EGFP with the 488 nm line of an argon laser, and the narrowest bandpass filter (505−530 nm) was employed for emission. DsRed2-ER was excited with the 543 nm line of a He−Ne laser, and emission was detected through a long-pass filter (emission above 560 nm). Zeiss LSM 510 software (Carl Zeiss, Inc.) was used to control the image acquisition parameters. All images were acquired at high resolution (1024 × 1024).

Fluorescence Microscope Imaging and Its Quantification. BHK-21 cells were imaged 1−3 days following transfection with GFP variants. A Nikon TE200 microscope running Metafluor software (Universal Imaging) with dual excitation capability was used for the cell imaging experiments (*46*). The ratio of fluorescence emission of EGFP-based Ca^{2+} sensors (measured at 510 nm) in response to excitation wavelengths of 385 and 480 nm was measured to monitor changes in $[Ca^{2+}]_{ER}$ in time series experiments. The $[Ca^{2+}]_{ER}$ in BHK-21 cells was quantified according to eq 7:

$$[Ca^{2+}] = K_d\left(\frac{R - R_{min}}{R_{max} - R}\right)^{1/n} \quad (7)$$

where R is the fluorescent emission ratio (measured at 510 nm) for 385 nm to 480 nm excitation in the initial state, R_{min} is the minimum of the emission ratio determined in the Ca^{2+}-free state, R_{max} is the maximum of the emission ratio in the Ca^{2+}-saturated state, K_d is the apparent dissociation constant (millimolar), and n is the Hill coefficient ($n = 1$). Ca^{2+}-free and Ca^{2+}-saturated states were obtained with cells treated with 5 μM ionomycin and exposed to 1.0 mM EGTA and 1.0 mM Ca^{2+}, respectively.

RESULTS

Design of EGFP-Based Ca^{2+} Sensors with a Single Inserted Ca^{2+}-Binding Motif. Figure 1 illustrates the design of Ca^{2+} sensors made by grafting a Ca^{2+}-binding motif, a combination of CaM loop III and its flanking helices, into EGFP based on the following criteria. First, Ca^{2+}-binding motifs such as loop III or intact EF-hand motif III from CaM were used to create Ca^{2+}-binding sites in EGFP. Ca^{2+} is chelated by 12 residues in the EF-hand motif. To the best of our knowledge, peptide fragments of an EF-hand motif of CaM have not been reported to interact with any CaM target enzymes, thereby producing a sensor that is unlikely to interfere with cellular signaling events. Our previous studies have shown that the Ca^{2+} binding affinity of the grafted loop can be varied by modifying charged residues in the loop and flanking helices (*47*, *48*), providing a convenient method for altering the Ca^{2+} binding affinity of any designed sensor. Second, the locations in EGFP where the Ca^{2+}-binding motif is grafted should be in a solvent-exposed loop region and have good solvent accessibility to enable rapid Ca^{2+} binding. Ideally, grafting of the Ca^{2+}-binding motif should not impact the protein folding and chromophore functionality. Third, to generate a Ca^{2+}-induced change in the optical signal following Ca^{2+} binding, the graft location should enable efficient Ca^{2+}-induced signal transfer from the grafted Ca^{2+}-binding motif to the fluorescent chromophore.

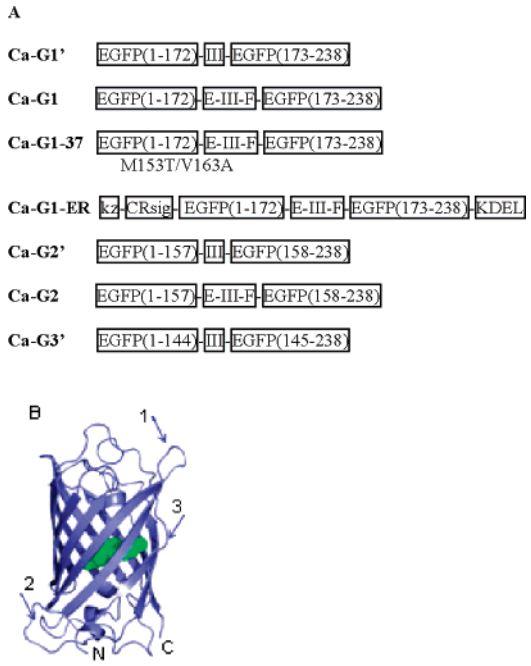

FIGURE 1: Model structure of EGFP-based Ca^{2+} sensors based on PDB entry 1ema. All Ca^{2+} sensors are composed of a Ca^{2+}-binding motif grafted into enhanced green fluorescent protein (EGFP). (A) Domain structure of GFP variants used for expression and imaging experiments. CRsig, calreticulin signal peptide (MLLSVPLLLGLLG-LAAAD); KDEL, ER retention signal; kz, Kozak consensus sequence for optimal translational initiation in mammalian cells. Note that constructs Ca-G1 and Ca-G2 contain the flanking sequences whereas Ca-G1′, Ca-G2′, and Ca-G3′ were designed without flanking sequences. (B) Schematic topology of grafting locations Glu172-Asp173 (position 1), Gln157-Lys158 (position 2), and Asn144-Tyr145 (position 3) in EGFP using PyMol version 0.98 (Delano Scientific LLC).

According to these criteria and previous mutation or permutation studies, three grafting sites were selected: Glu172-Asp173 within loop 9 of EGFP (position 1), Gln157-Lys158 within loop 8 (position 2), and Asn144-Tyr145 within loop 7 (position 3). Loop III of CaM, with or without the flanking helices, was used as a Ca^{2+}-binding motif and grafted at these positions to construct EGFP-based Ca^{2+} sensors (Figure 1A). Next, M153T and V163A mutations were inserted into construct Ca-G1 to create a sensor with improved expression at 37 °C (Ca-G1-37) (*41*, *42*). Finally, a construct with both the ER targeting sequence and the retention sequence, which specifically targets Ca-G1 to the ER of mammalian cells, was designed and is termed Ca-G1-ER.

Spectroscopic Properties of EGFP-Based Ca^{2+} Sensors and Sensitive Locations of EGFP. Spectroscopic properties of Ca^{2+} sensors were first investigated using purified proteins (pH 7.4). Panels A and B of Figure 2 show the visible absorbance and fluorescence emission spectra, respectively, of EGFP-wt and different Ca^{2+} sensor constructs. The spectroscopic properties, including extinction coefficients and quantum yields, of Ca^{2+} sensors are summarized in Table 1. The insertion of loop III of CaM at Gln157-Lys158 of EGFP [Ca-G2′ and Ca-G2 (only Ca-G2′ is shown in Figure 2A,B) (Figure 1A)] resulted in a protein with spectroscopic

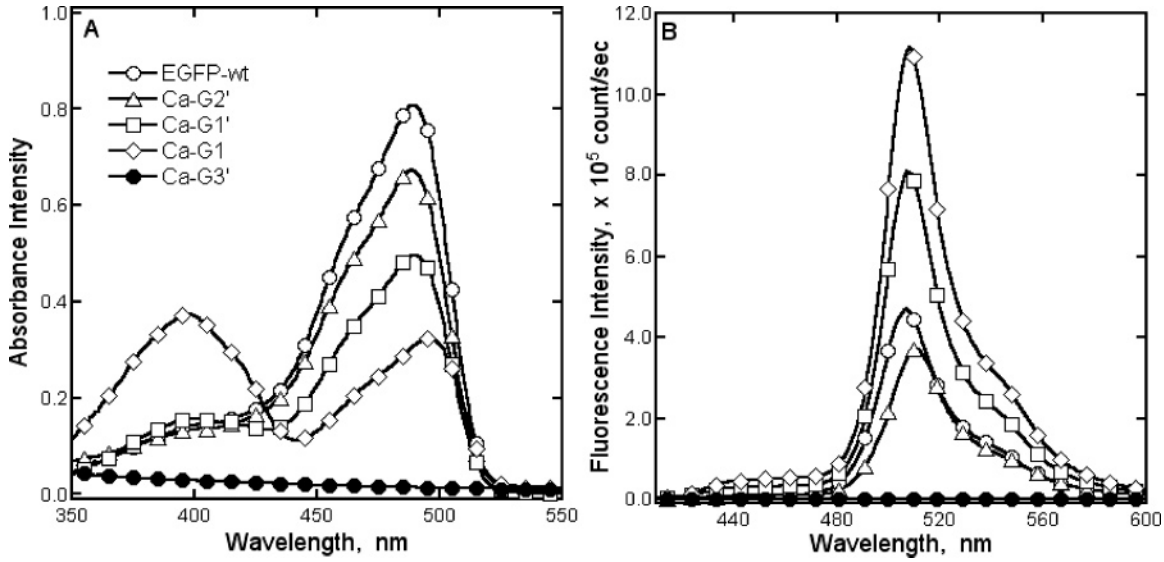

FIGURE 2: Visible absorbance (A) and fluorescence (B) spectra of EGFP-wt and its variants. The measurements were performed in 10 mM Tris and 1 mM DTT (pH 7.4). The protein concentrations were 20 and 10 μM for absorbance and fluorescence experiments, respectively. The length of the cuvette was 10 mm. The fluorescence experiments were performed with a slit width of 1 nm for both excitation and emission. $\lambda_{ex} = 398$ nm. Symbols of EGFP-wt and its variants in panel B are the same as those in panel A.

Table 1: Spectroscopic Properties of EGFP and Ca^{2+} Sensor Constructs

	ϵ (398 nm)[a]	ϵ (490 nm)	ϵ (490 nm)/ϵ (398 nm)	quantum yield
EGFP[b]	9.8	55.9	5.7	0.60
Ca-G1′	10.9	34.4	3.2	0.53
Ca-G1	25.9	21.5	0.8	0.59
Ca-G2′	9.3	46.4	5.0	0.60
Ca-G2	8.5	38.6	4.5	0.69
Ca-G3′[c]	N/A[d]	N/A[d]	N/A[d]	N/A[d]

[a] ϵ is the extinction coefficient in units of 10^3 M^{-1} cm^{-1}. The wavelengths in absorption peaks are given in parentheses. [b] EGFP-wt was used as a reference in the calculation of absorbance extinction coefficient (ϵ) and fluorescent quantum yield of EGFP variants. [c] The chromophore was not formed in Ca-G3′. [d] Not available.

properties similar to those of EGFP-wt with a slight decrease in absorbance intensity. Note that the major absorbance peak at 490 nm and minor absorbance peak at 398 nm reflect the relative population of anionic and neutral states of the chromophore. Figure 2B shows that excitation at 398 nm (the neutral state) contributed greatly to the emission peak at 510 nm. As summarized in Table 1, the constructs with a Ca^{2+}-binding motif grafted at Gln157-Lys158 (position 2) (Ca-G2′ and Ca-G2) had spectroscopic properties (extinction coefficients and quantum yield constants at both 398 and 490 nm) similar to those of EGFP-wt. Strikingly, grafting loop III of CaM at Glu172-Asp173 of EGFP (Ca-G1′) resulted in the formation of a protein which exhibited a slight increase in absorbance at 398 nm and a decrease in absorbance at 490 nm compared to EGFP-wt. Moreover, the insertion of loop III containing the flanking EF-helices at the same location (Ca-G1) resulted in a protein which had a further increase in absorbance at 398 nm and a decrease at 490 nm. The extinction coefficients of Ca-G1 were increased 2.6-fold at 398 nm and decreased ~60% at 490 nm compared to those of EGFP-wt. Concurrently, a corresponding increase in fluorescence emission was observed for both Ca-G1′ and Ca-G1 (Figure 2B). In contrast, the chromophore was not formed after insertion of loop III at Asn144-Tyr145 of EGFP (Ca-G3′), indicated by the lack of green fluorescence in the bacterial expression as well as in the purified protein. Thus, the grafting of a Ca^{2+}-binding motif at Glu172-Asp173 in EGFP significantly shifts the population of the chromophore from the anionic state as indicated by the 490 nm peak to the neutral state as indicated by the 398 nm peak. It is likely that Glu172-Asp173 of EGFP is a chromophore sensitive location.

CD analysis was performed to test whether the changes in the chromophore properties of the Ca^{2+} sensor constructs were due to structural changes. All Ca^{2+} sensor constructs exhibited CD spectra similar to that of EGFP-wt (Figure S1 of the Supporting Information), suggesting that the insertion of a Ca^{2+}-binding motif into EGFP did not significantly change the folding of the β-sheet structure of GFP. Next, we examined the pH sensitivity of the optical properties of Ca-G1′, since a few GFP-based biosensors have been reported to be pH sensitive. Figure S2 shows the absorbance spectra of Ca-G1′ as a function of pH. Changing the pH from 9.0 to 5.0 resulted in an increase in the absorbance at 398 nm and a decrease in the absorbance at 488 nm. The pK_a of Ca-G1′ is 7.45 $\pm$ 0.05, whereas the pK_a of EGFP is 6.0 (*49*). These data suggest that the optical properties of the designed Ca^{2+} sensor are more sensitive to pH at the physiological pH than those of EGFP-wt. Caution to maintain pH value when applying our sensor to measure calcium responses should be taken.

Effect of Ca^{2+} Binding on Spectroscopic Properties of EGFP-based Ca^{2+} Sensors. As shown in Figure 3A, an increase in absorbance at 398 nm concomitant with a decrease at 490 nm was observed in response to the addition of Ca^{2+} to Ca-G1-37. Similarly, Ca^{2+} binding resulted in an increase in fluorescence with excitation at 398 nm (Figure 3B) and a decrease with excitation at 490 nm (Figure 3C). The dynamic range value was 1.8 and was calculated by dividing the fluorescence emission ratio excited at 398 and 490 nm of the Ca^{2+}-saturated state (R_{max}) by that of the Ca^{2+}-free state (R_{min}) (see Materials and Methods). Figure 3D shows the fluorescence emission ratio, F_{398nm}/F_{490nm}, of Ca-G1-37 as a function of Ca^{2+} concentration. The normalized

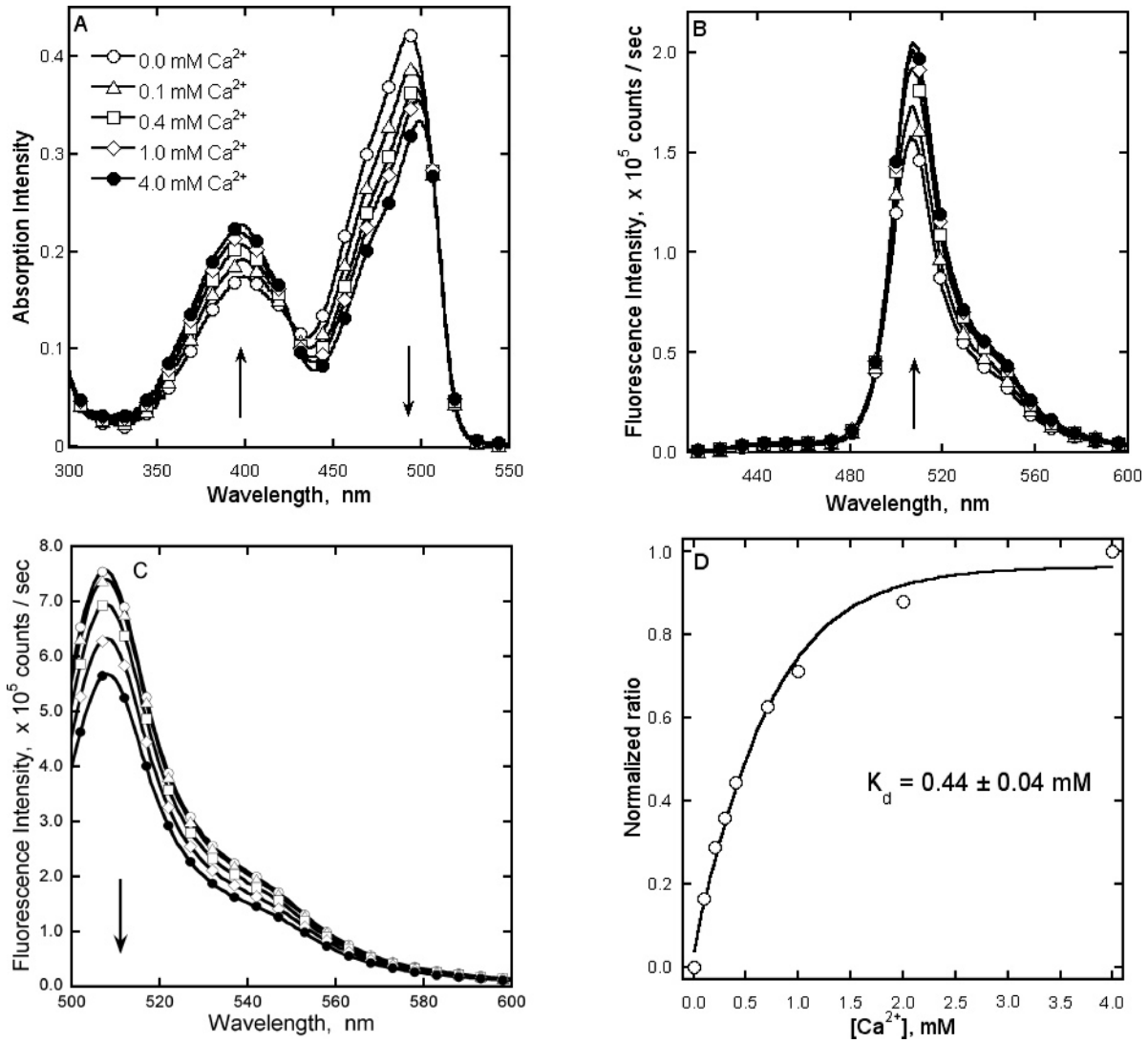

FIGURE 3: Spectroscopic characterization of Ca^{2+} sensor Ca-G1-37. (A) Visible absorption spectrum for sensor Ca-G1-37 with increasing Ca^{2+} concentrations. Ca^{2+} dependence of fluorescence emission spectra with excitation λ_{ex} of 398 (B) and 490 nm (C). Symbols for different Ca^{2+} concentrations in panels B and C are same as those in panel A. The measurements were performed at 17 μM Ca-G1-37 for visible absorption and 1.7 μM Ca-G1-37 for fluorescence experiments with 10 mM Tris and 1 mM DTT (pH 7.4), respectively. The slit widths of excitation and emission were 1 and 2 nm, respectively. The arrows indicate the direction of signal change resulting from an increase in the Ca^{2+} concentration. (D) Normalized F_{398nm}/F_{490nm} ratio curve fitting of the Ca^{2+} titration data.

fluorescence emission ratio change could be fitted as a 1:1 Ca-G1-37−Ca^{2+} complex (eq 2), yielding an apparent dissociation constant (K_d = 0.44 ± 0.04 mM) for its Ca^{2+} binding affinity. The Ca^{2+} binding affinity of EGFP-based Ca^{2+} sensors was also determined using a rhodamine-5N competition titration approach. The Ca^{2+} binding affinities of these Ca^{2+} sensors varied from 0.4 to 2 mM (Table 2), as determined by different techniques. These values agreed well with the approximate Ca^{2+} concentration found in cellular compartments such as the ER (*4*, *6*, *7*), making these Ca^{2+} sensors promising candidates for physiological experiments in living cells.

Ca^{2+} Selectivity of the EGFP-Based Ca^{2+} Sensor. We next examined the binding selectivity of our developed Ca^{2+} sensors for Ca^{2+} in experiments in which various other metal ions were used in a competition binding assay. Thus, the binding selectivity of our developed Ca^{2+} sensors for Ca^{2+} was examined by measuring the change in the ratio F_{398nm}/F_{490nm} in the presence of 1.0 mM Ca^{2+} before and following the addition of various metal ions. In cells, total metal concentrations for Cu^{2+}, Zn^{2+}, and Mg^{2+} are estimated to be ~10 μM, ~0.1 mM, and >10 mM, respectively. However, the free levels of these metal ions are significantly lower than the total concentrations, which protects the cell

Table 2: Comparison of Ca^{2+} Binding Affinities of Different EGFP-Based Ca^{2+} Sensors

	Ca^{2+} binding affinity, K_d (mM)	
	Ca^{2+} titration	rhodamine-5N competitive titration
Ca-G1′	2.0 ± 0.4	0.9 ± 0.2
Ca-G1	0.8 ± 0.1[a]	0.4 ± 0.1
	0.8 ± 0.1[b]	
	0.6 ± 0.1[c]	
Ca-G1-37	0.44 ± 0.04	0.2 ± 0.1
Ca-G2′	N/A[d]	0.8 ± 0.2
Ca-G2	N/A[d]	0.2 ± 0.1
Ca-G3′	N/A[d]	0.7 ± 0.2

[a] Estimated with results from a fluorescence spectrophotometer. [b] Estimated by fitting Scheme 1 to results from the stopped-flow spectrofluorimeter. [c] Estimated by fitting normalized changes (Amp) of the stopped-flow spectrofluorimeter. [d] Not available.

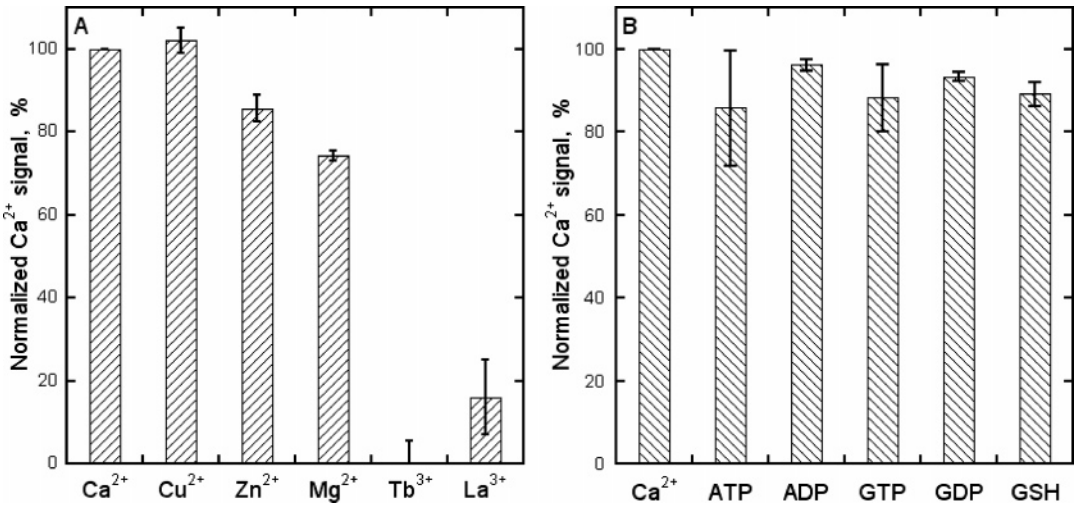

FIGURE 4: Ca^{2+} responses of Ca-G1-37 in the presence of different metal ions (A) Cu^{2+} (0.1 μM), Zn^{2+} (0.1 mM), Mg^{2+} (10.0 mM), Tb^{3+} (5.0 μM), and La^{3+} (5.0 μM) and the intracellular molecules (B) ATP (0.2 mM), ADP (0.2 mM), GTP (0.1 mM), GDP (0.1 mM), and GSH (1.0 mM). The ratio of fluorescence emission of Ca-G1-37 with 398 and 490 nm excitation in the presence of 1.0 mM Ca^{2+} was used to normalize the values obtained with the other metals or intracellular molecules using eq 5. The measurements were performed using 1.7 μM Ca-G1-37 with 10 mM Tris and 1 mM DTT (pH 7.4). Excitation and emission slit widths were 1 and 2 nm, respectively.

against potentially toxic reactions (*50*). For example, intracellular free copper is not detected, and copper chaperone is used in vivo to allocate copper to its target proteins directly (*51*). Figure 4A shows the Ca^{2+} responses of sensor Ca-G1-37 in the presence of Cu^{2+}, Zn^{2+}, Mg^{2+}, Tb^{3+}, and La^{3+}. Note that no effect of Cu^{2+} (0.1 μM) on the fluorescence response of the sensor for Ca^{2+} was observed (101.95 $\pm$ 3.02% compared to the reference value of 100% for 1.0 mM Ca^{2+}). Zn^{2+} (0.1 mM) and Mg^{2+} (10.0 mM) produced only a small change in the fluorescence response (reduction to 85.71 $\pm$ 3.34 and 74.29 $\pm$ 1.22%, respectively). Nonphysiological metal ions, such as Tb^{3+} (5.0 μM) and La^{3+} (5.0 μM), have metal coordination properties similar to those of Ca^{2+} and are able to compete more strongly with Ca^{2+} responses of the sensor (0.15 $\pm$ 5.4 and 16.0 $\pm$ 9.0%, respectively). These results suggest that the developed Ca^{2+} sensor, Ca-G1-37, has good metal selectivity for Ca^{2+}, La^{3+}, and Tb^{3+} and only a lower degree of selectivity for the other physiological metal ions.

The effects of small molecules, including adenosine triphosphate (ATP), adenosine diphosphate (ADP), guanosine triphosphate (GTP), guanosine diphosphate (GDP), and glutathione (GSH), on the Ca^{2+} response of EGFP-based Ca^{2+} sensors were also analyzed by measuring the change in the ratio F_{398nm}/F_{490nm} in the presence of 1.0 mM Ca^{2+} before and following their addition. Figure 4B indicates that the addition of ATP (0.2 mM), ADP (0.2 mM), GTP (0.1 mM), GDP (0.1 mM), and GSH (1.0 mM) resulted in only a small decrease in the fluorescence response (reduction to 85.75 $\pm$ 13.98, 96.17 $\pm$ 1.36, 88.30 $\pm$ 8.09, 93.29 $\pm$ 1.01, and 89.18 $\pm$ 2.90%, respectively). These results indicate that the developed Ca^{2+} sensor, Ca-G1-37, has a high Ca^{2+} binding affinity to compete with small molecules, including ATP, ADP, GTP, GDP, and GSH, in the intracellular environment.

Kinetics of Binding of Ca^{2+} to the EGFP-Based Ca^{2+} Sensor. As shown in Figure 5A, mixing Ca-G1 with various concentrations of Ca^{2+} resulted in a rapid increase in the fluorescence emission at 510 nm with excitation at 398 nm. The change in the fluorescence signal is consistent with a single-exponential function (eq 6) yielding observed rates for fluorescence emission change (k_{obs}) and amplitudes (Amp). As shown in Figure 5B, the k_{obs} values of Ca-G1 decreased with an increase in the concentration of Ca^{2+}, consistent with the kinetic model of Scheme 1, in which Ca^{2+} rapidly associates with one species of Ca-G1 that is in equilibrium with a second form of the biosensor. The increases in fluorescence emission excited at 398 nm of Ca-G1 observed upon Ca^{2+} binding as shown in Figure 5A further suggest that the neutral form of Ca-G1 is the species that binds Ca^{2+} (E** in Scheme 1), whereas the anionic form of the biosensor (E*) does not bind Ca^{2+}. According to this kinetic model, k_1 is the first-order rate constant (s^{-1}) for the conversion of the anionic species to the neutral species of Ca-G1, k_2 is the first-order rate constant (s^{-1}) for the conversion of the neutral species to the anionic form of Ca-G1, and K_{d2} represents the apparent dissociation constant for the binding of Ca^{2+} to the neutral form of Ca-G1 (mM).

By fitting k_{obs} values determined as a function of Ca^{2+} concentration to eq 8, we estimated the k_1 and k_2 values to be 9.5 $\pm$ 0.3 and 14.0 $\pm$ 0.6 s^{-1}, respectively, and a K_{d2} value of 0.8 $\pm$ 0.1 mM was determined. The K_{d2} value was independently estimated to be 0.6 $\pm$ 0.1 mM by fitting the normalized amplitude in fluorescence emission as a function of the concentration of Ca^{2+} by using eq 2 (Figure 5C). Within errors associated with the measurements, the K_d values determined using stopped-flow fluorescence spectroscopy are in agreement with the K_d value independently determined in static titrations using a spectrofluorometer, which yielded a K_d value of 0.8 $\pm$ 0.1 mM (Table 2). This, in turn, strongly supports the validity of the proposed minimal kinetic mechanism of Scheme 1 for binding of Ca^{2+} to Ca-G1, where rates of fluorescence changes associated with binding of Ca^{2+} to the neutral species of Ca-G1 reflect rates of interconversion of the neutral and anionic forms of Ca-G1, as compared to the rapid association and dissociation of Ca^{2+} with and from the biosensor.

$$k_{obs} = k_1 + k_2\left(\frac{K_{d2}}{K_{d2} + [Ca^{2+}]}\right) \quad (8)$$

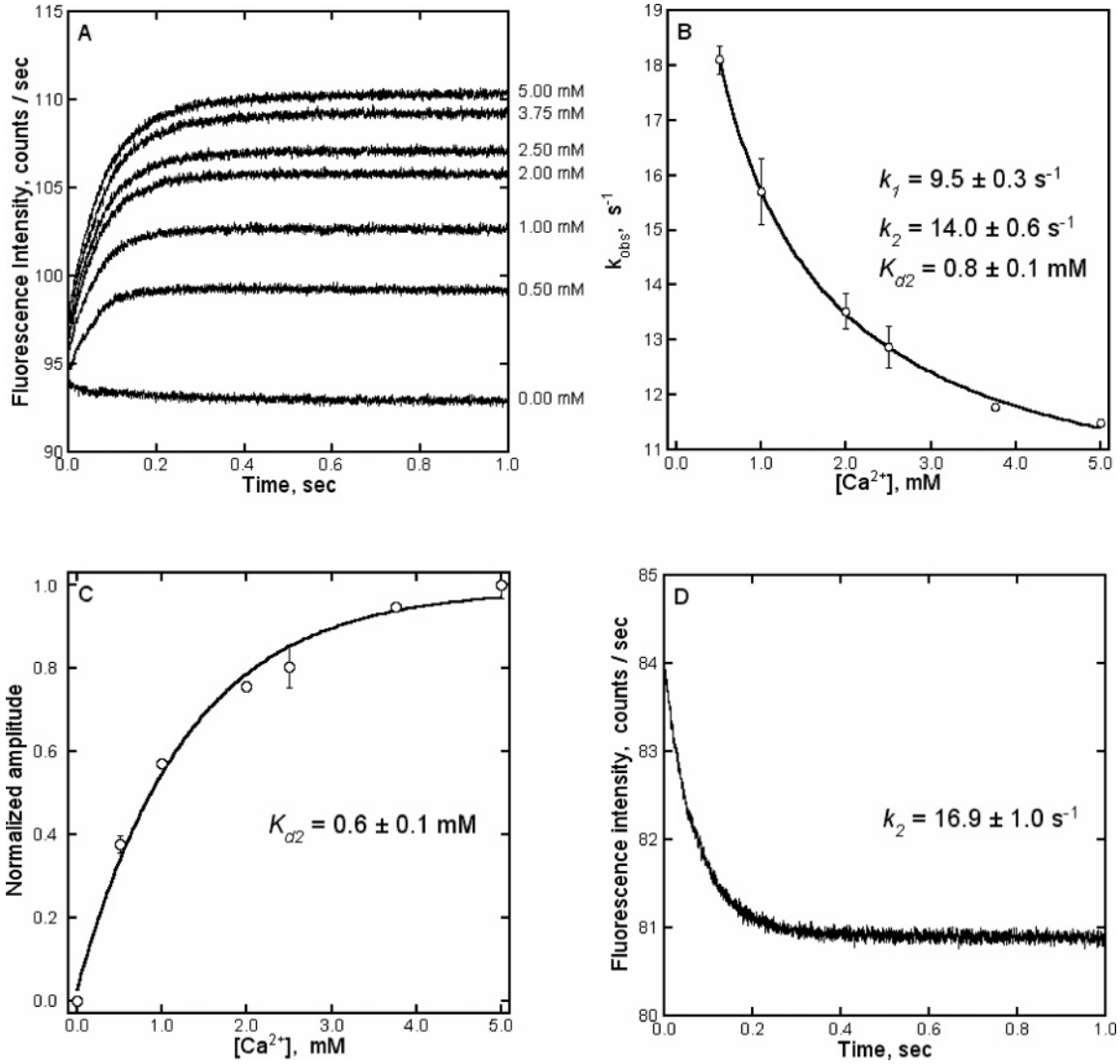

FIGURE 5: Kinetic analysis of association of Ca^{2+} with Ca-G1. (A) Stopped-flow traces of fluorescence increase (λ_{ex} = 398 nm) upon rapid mixing of Ca-G1 at a final concentration of 20 μM with Ca^{2+} at different concentrations. (B) Observed rates of fluorescence increases as a function of Ca^{2+} concentration. (C) Maximal changes in the amplitude of the fluorescence intensities observed in panel A as a function of Ca^{2+} concentration. (D) Stopped-flow trace of fluorescence decrease (λ_{ex} = 398 nm) upon rapid mixing of 40 μM Ca-G1 preloaded with 0.8 mM Ca^{2+} with Tris buffer. All measurements were carried out in 10 mM Tris and 1 mM DTT (pH 7.4) at 25 °C. A 455 nm long pass filter was used to collect the emission with a main peak at 510 nm. Data were fit to eqs 6 (A and D), 8 (B), and 2 (C).

Scheme 1

$$E* \underset{k_2}{\overset{k_1}{\rightleftharpoons}} E** \underset{K_{d2}}{\overset{Ca^{2+}}{\rightleftharpoons}} Ca^{2+} - E**$$

According to the minimal kinetic mechanism of Scheme 1 and the data shown in Figure 5A, the release of Ca^{2+} from preloaded Ca-G1 is expected to be associated with a decrease in fluorescence whose rate of fluorescence change represents the slow rate of conversion from the neutral to the anionic form of Ca-G1, i.e., k_2. Consequently, stopped-flow spectroscopy was utilized to independently determine k_2 by mixing equal volumes of Ca^{2+}-saturated sensor with 10 mM Tris and 1 mM DTT (pH 7.4). As expected, the fluorescence intensity at 510 nm decreased following Ca^{2+} release, and the time course of fluorescence change was consistent with a single-exponential process (eq 6). As shown in Figure 5D, a k_{obs} value of 16.9 ± 1.0 s^{-1} was estimated in this experiment by fitting the data to eq 6, in good agreement with the value of 14 ± 0.6 s^{-1} determined for k_2 from the data in Figure 5B. Together, the kinetic data support the conclusion that Ca^{2+} rapidly associates with and dissociates from the neutral form of Ca-G1, yielding a change in the relative amounts of neutral and anionic species that are associated with a change in the intensity of the fluorescence signal from Ca-G1.

Monitoring ER Ca^{2+} Responses in Cells. Localization of the Ca^{2+} sensor, Ca-G1-ER, was confirmed in HeLa cells by cotransfecting the cells with the ER marker DsRed2-ER that has been shown to localize exclusively to this region in mammalian cells (*39*, *52*). Figure 6 shows images taken through the green (A, Ca-G1-ER) and red (B, DsRed2-ER) channels which were excited at 488 and 543 nm, respectively. The yellow color seen in the merged image (Figure 6C) indicates the complete colocalization of Ca-G1-ER with the ER marker DsRed2-ER in the ER of HeLa cells. Figure 6D shows the ER distribution of Ca-G1-ER in a BHK-21 cell, a mammalian fibroblast cell line. Note the same granular distribution of Ca-G1-ER in panels A and D of Figure 6, suggesting that the Ca^{2+} sensor also specifically localizes to

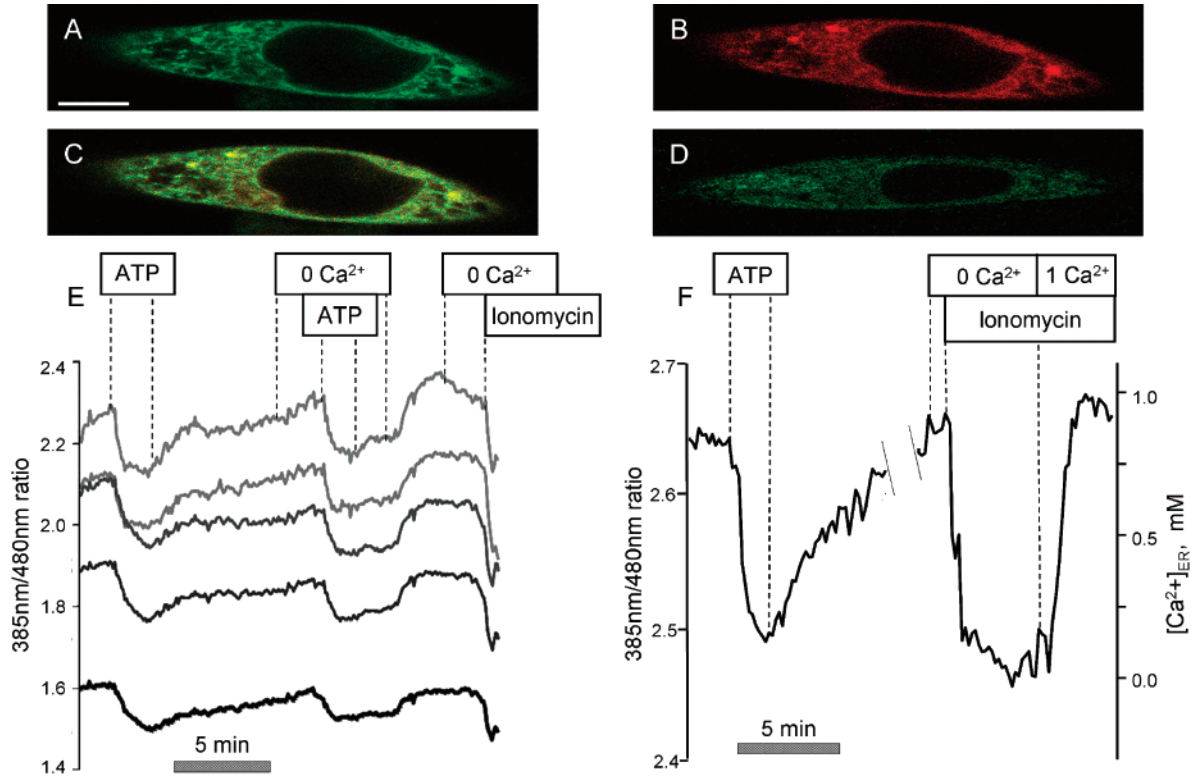

FIGURE 6: Localization of the sensor Ca-G1-ER in two cell types (HeLa and BHK-21 cells) and Ca response of this sensor in BHK-21 cells. Localization of Ca-G1-ER (A) and DsRed2-ER (B) and overlay of Ca-G1-ER and DsRed2-ER in HeLa cells (C). Localization of Ca-G1-ER in BHK-21 cells (D). Confocal images of Ca-G1-ER and DsRed2-ER localization were performed with the 488 nm line of an argon laser for the green channel and the 543 nm line of a He−Ne laser for the red channel using a 100× oil immersion objective. The scale bar indicates 10 μm in panels A−D. Time course of Ca^{2+} responses in the ER of BHK-21 cells in response to different treatments (E) and pseudocalibration of Ca^{2+} concentrations in the ER (F). The time course of the Ca^{2+} signal response was expressed as the fluorescence emission ratio at 510 nm for excitation at 385 and 480 nm on a Nikon TE200 microscope running Metafluor software (Universal Imaging). The left-hand ordinate represents the 510 nm fluorescence emission ratio (excitation at 385 and 480 nm) in both panels E and F, and the right-hand ordinate represents the calibrated Ca^{2+} concentration in the ER in panel F.

the ER of BHK cells. In contrast, Ca-G1, which lacked the ER signal peptides, was expressed diffusely throughout the cytoplasm of the cells, thereby serving as a negative control (data not shown).

BHK-21 cells have been used previously to investigate the physiological roles of $[Ca^{2+}]_{ER}$ in intact cells by using small, low-affinity Ca^{2+} indicators (*46*, *53*). ATP (100 μM) is a Ca^{2+}-mobilizing agonist of this cell type and elicits release of Ca^{2+} from the ER through Ins(1,4,5)P_3-mediated pathways. As shown in Figure 6E, the addition of ATP (100 μM) resulted in a significant decrease (7.3 ± 0.6% relative change) in the fluorescence ratio measured at 510 nm (excitation at 385 and 480 nm). The experiment shows five representative cells imaged in the same experiment, and the results are typical of results obtained in five independent experiments. This decrease in $[Ca^{2+}]_{ER}$ was also observed following application of ATP in Ca^{2+}-free buffer, suggesting that ATP released Ca^{2+} from the ER in a manner independent of extracellular Ca^{2+}. The refilling of the Ca^{2+} store required several minutes in the presence of a normal extracellular Ca^{2+} concentration in the medium. Similarly, the addition of the Ca^{2+} ionophore, ionomycin, under Ca^{2+}-free conditions significantly emptied the ER store as indicated by the decreased 385 nm to 480 nm fluorescence ratio. To obtain an estimate of $[Ca^{2+}]_{ER}$, a pseudocalibration was performed in BHK-21 cells using eq 7 and a K_d of 0.8 mM for Ca-G1 as shown in Table 2 (Figure 6F). The 385 nm to 480 nm fluorescence ratio decreased to a minimum value (R_{min}) following a wash with Ca^{2+}-free medium (EGTA) and the subsequent addition of ionomycin (~5 μM) to the Ca^{2+}-free medium (estimated to contain less than 10 nM Ca^{2+} using the freeware program "Bound and Determined"). The addition of a millimolar extracellular concentration of Ca^{2+} (~1 mM) resulted in a large increase in the magnitude of the Ca^{2+} signal with a plateau that approached the saturation state with a maximum of the 385 nm to 480 nm fluorescence ratio (R_{max}). The initial Ca^{2+} concentration in the ER of the BHK-21 cell was estimated to be less than 1 mM using eq 7, and addition of ATP (100 μM) reduced $[Ca^{2+}]_{ER}$ to approximately 0.15 mM (Figure 6F). As expected, no significant fluorescence signal change was observed in response to the experimental protocol described above in cells transfected with the wild-type control construct, EGFP-wt-ER (data not shown). These imaging experiments demonstrate the usefulness of this novel class of Ca^{2+} sensors in living cells, and we anticipate that their future application will facilitate the investigation of the role of the ER in Ca^{2+} signaling and Ca^{2+} homeostasis.

DISCUSSION

Creating Ca^{2+} Binding EGFP Variants. We have shown previously that when continuous Ca^{2+} binding motifs are grafted into non-Ca^{2+}-binding host proteins, such as the cell adhesion protein CD2, the Ca^{2+}-binding motifs maintain their native Ca^{2+} binding properties (*54*, *55*). This grafting approach has been applied to study isolated EF-hand motifs

and to estimate their cooperativity (*47*, *48*). The Ca^{2+} binding affinity of these motifs can be changed by varying the length of the glycine linker, attaching flanking helices, and changing the number of charged residues in the EF-hand loop. In this study, we demonstrate that the Ca^{2+}-binding motif grafted into EGFP also binds Ca^{2+} and that the Ca^{2+} binding affinity of this motif can be altered several-fold (with K_d ranging from 0.4 to 2 mM) depending on the presence or absence of flanking helices. Our results clearly demonstrate that EGFP-based sensors with different Ca^{2+} binding affinities can be created by this grafting approach. Affinities of these sensors are very similar to those of Ca^{2+} binding proteins found in the ER and the extracellular environment. For example, Ca^{2+} binding proteins in the ER have a low Ca^{2+} binding affinity corresponding to the submillimolar free resting Ca^{2+} concentration in the ER lumen. Calreticulin, one of the most prominent Ca^{2+} binding proteins in the ER lumen, binds Ca^{2+} with low affinity and high capacity ($K_d = 2$ mM, $B_{max} = 25$ mol of Ca^{2+}/mol of protein) (*56*). Using a competitive assay, we have also demonstrated that the developed Ca^{2+} sensor has a good metal selectivity for Ca^{2+} over other physiological metal ions. Furthermore, the existence of small molecules, including ATP, ADP, GTP, GDP, and GSH, does not alter the Ca^{2+} sensing capability of the developed sensor.

Developing Ca^{2+} Sensors at Chromophore Sensitive Locations of a Fluorescent Protein. As shown in Figure 2, the grafting of a Ca^{2+}-binding motif into three different locations of EGFP results in different effects on the EGFP chromophore properties. Grafting the Ca^{2+}-binding motif at Asn144-Tyr145 (Figure 1) resulted in a lack of chromophore formation, although the same site in the enhanced yellow fluorescent protein, EYFP, has been used to fuse CaM or a zinc finger domain to newly introduced termini (*33*, *57*). Grafting at Gln157-Lys158 had only a small effect on the chromophore properties, as this construct had extinction coefficients and quantum yield constants similar to those of EGFP-wt (Table 1). While previous studies have inserted either a pentapeptide (*58*), a hexapeptide (*59*), TEM1 β-lactamase (*60*), CaM, or a zinc finger domain at either Glu172-Asp173 or Gln157-Lys158 (*33*), no detailed characterization of the effect on the chromophore properties was reported. Grafting Ca^{2+}-binding motifs between Glu172 and Asp173 of EGFP, which is located ~20 Å from the chromophore, significantly altered the chromophore properties with an increase in the absorption spectrum at 398 nm and a decrease at 490 nm (Figure 2A). Concurrently, there was a significant increase in the fluorescence emission at 510 nm with excitation at 398 nm. These changes suggest that grafting a Ca^{2+}-binding motif between Glu172 and Asp173 of EGFP-wt shifts the chromophore equilibrium from the anionic to the neutral state. Further, Ca^{2+} binding resulted in an increase in the absorption spectra at 398 nm and a decrease at 490 nm (Figure 3A). Such changes in spectral properties permit ratiometric measurements of Ca^{2+} concentrations using the fluorescence emission ratio monitored at 510 nm for excitation at 398 and 490 nm. Clearly, binding of Ca^{2+} to Ca-G1 promotes the protonation of the anionic form of this construct and increases the proportion of the neutral form of the chromophore (Figure 1B). While the grafting location of the Ca^{2+}-binding motif at Glu172-Asp173 is not in the immediate neighboring environment of the chromophore, it nevertheless has a significant effect on the local conformation of the chromophore without disturbing the packing and folding of the protein. It is possible that Ca^{2+} binding results in a change in the local environment of the chromophore, stabilizing it in the neutral state.

Rate Constants Associated with Ca^{2+} Binding and Dissociation. Binding of Ca^{2+} to Ca-G1 results in a rapid shift of the chemical equilibrium of the chromophore between its anionic and neutral states (Scheme 1). This conclusion is supported by visible absorption, fluorescence emission, and stopped-flow fluorescence data. Both kinetic and thermodynamic parameters, including the forward and reverse rate constants for the interconversion of the anionic and neutral states of the chromophore, as well as the apparent dissociation constant for binding of Ca^{2+} to Ca-G1 were determined using stopped-flow fluorescence measurements. This approach established that the rates of association and dissociation of Ca^{2+} with and from the sensor must be significantly larger than both the forward and reverse first-order rate constants that define the chemical equilibrium of the chromophore (k_1 and k_2, respectively, in Scheme 1), which are between ~10 and ~20 s^{-1}. The rate of association of Ca^{2+} with proteins is generally a diffusion-limited process with an on-rate (k_{on}) equal or greater than 1×10^6 M^{-1} s^{-1} (*36*). Since the apparent dissociation constant for the Ca^{2+} binding process determined in this study for Ca-G1 is ~0.8 mM for Ca-G1, an off-rate (k_{off}) of ~800 s^{-1} can be estimated from the equation $k_{off} = k_{on}K_d$. Whereas the on-rate of GFP-based Ca^{2+} sensors is generally not the limiting factor in Ca^{2+} measurements, the slow off-rate exhibited by Ca^{2+} sensors limits their usefulness in monitoring changes in Ca^{2+} concentration in vivo, especially for fast Ca^{2+} oscillations (*32*, *36*). To overcome this limitation, an improvement of the off-rate constant (k_{off}) to 256 s^{-1} was obtained by redesigning the binding interface between calmodulin and its targeting peptide in GFP-based Ca^{2+} sensors (*32*). Optimizing the protonation rate of the chromophore in GFP-based Ca^{2+} sensors will provide a means of enhancing further the accuracy with which Ca^{2+} signals can be measured with high temporal resolution.

Ca^{2+} Responses in the ER. To understand the role of the ER in Ca^{2+} signaling, many innovative studies have been conducted. Both ratiometric dyes such as Mag-fura-2 and nonratiometric dyes such as Mag-fluo-4 with Ca^{2+} binding affinities of ~50 μM have been used to measure the intraluminal Ca^{2+} concentration in the ER (*53*, *61*−*63*). Hofer and colleagues were the first to report an estimate of the Ca^{2+} concentration in the ER of BHK-21 cells, 188 ± 21 μM (*27*). Pozzan and colleagues directly monitored the free Ca^{2+} concentration in both the ER and the SR by targeting the Ca^{2+} sensitive photoprotein aequorin to these compartments in cultured skeletal muscle myotubes and estimated the Ca^{2+} concentration to be approximately 200 μM (*64*). The agonist-induced Ca^{2+} response in the ER of HeLa cells was successfully monitored by Miyawaki et al. using GFP-pair Ca^{2+} sensors with different Ca^{2+} binding affinities, and $[Ca^{2+}]_{ER}$ was reported to be in the range of 60−400 μM (*31*). Later, a new generation of GFP-pair Ca^{2+} sensors, named D1, was developed using both modified CaM and its binding peptide to monitor Ca^{2+} oscillations in response to ATP in the ER of HeLa cells and to explore the effect of the antiapoptotic protein Bcl-2 on ER Ca^{2+} of MCF-7 breast cancer epithelial cells (*32*). We have shown here that the

EGFP-based Ca^{2+} sensor Ca-G1-ER is able to monitor $[Ca^{2+}]_{ER}$ in BHK-21 cells after stimulation of cells with agonists or the Ca^{2+} ionophore. The Ca^{2+} concentration in the ER of BHK cells was estimated to be less than 1.0 mM which is consistent with values reported previously (*27*, *31*, *32*, *64*).

Advantage of This New Class of Ca^{2+} Sensors Compared to Other GFP-Based Ca^{2+} Sensors. The fact that GFP and its derivatives are fluorescent and can be targeted easily to different cellular compartments has stimulated many efforts to develop GFP constructs as Ca^{2+} sensors in vivo. Generally, two series of GFP-based Ca^{2+} sensors have been developed. One is based on fluorescence resonance energy transfer (FRET) between two GFP variants following binding of Ca^{2+} to CaM, or more recently to TnC, resulting in the binding to a target peptide (M13 for CaM and TnI for TnC) and a subsequent change in distance between paired GFPs (*31*, *36*, *65*). Another series of GFP-based Ca^{2+} sensors has been constructed by the insertion of CaM and its targeting peptide at defined locations within a single GFP molecule. The resulting constructs exhibit a change in fluorescence signal following binding of Ca^{2+} (*66*). All such GFP-based Ca^{2+} sensors reported so far are based on a similar mechanism, namely, using natural Ca^{2+} binding proteins (e.g., CaM and TnC) to confer Ca^{2+} sensitivity to a GFP-based sensor. However, there are three important concerns and limitations related to the application of these Ca^{2+} sensors comprised of essential Ca^{2+} binding proteins and their binding partners (e.g., CaM binding peptides). First, CaM is a ubiquitous signaling protein in mammalian cells, and its concentration varies from several micromolar to millimolar levels depending on cell type and sublocations within cells (*34*, *67*, *68*). In the past few years, CaM has been reported to be associated with ion channels, pumps, and gap junctions, and dynamic changes in Ca−CaM complex levels are an integral part of cellular Ca^{2+} signaling (*69*−*71*). Since expression of a micromolar level of Ca^{2+} sensors is generally required for cell imaging (*72*) and this concentration is comparable to endogenous levels of CaM already present in the cell, this approach has the potential to interfere with Ca^{2+} signaling (*67*). It has been reported that the overexpression of CaM in transgenic mice results in severe cardiac hypertrophy (*73*). Thus, it is possible that perturbation and/or alteration of the existing Ca^{2+} signaling system in cells can result by the introduction of additional CaM and M13 peptides, or troponin C/I, as part of current Ca^{2+} sensors. Second, CaM is a versatile protein involved in the regulation of many important biological processes and has been found to associate with more than 300 different proteins (*69*, *74*, *75*). This class of GFP-based Ca^{2+} sensors suffers from competition with endogenous CaM or TnC and/or its numerous target proteins within living cells, reducing the dynamic range of this class of Ca^{2+} sensors (*76*−*78*). Because of these issues, numerous efforts have been made to increase the dynamic range and reduce the level of competition with endogenous proteins, including V68L and Q69K mutations in yellow fluorescent protein (YFP) (*79*), the modification of both CaM and its binding peptide (*32*, *34*), the insertion of CaM targeting peptides into CaM (*65*), replacement of YFP with its circularly permuted variant (cpYFP) or Venus (*35*, *38*), and the replacement of CaM with other Ca^{2+} binding proteins such as TnC (*36*, *37*). Third, the sensing capability of these sensors is dependent on conformational changes associated with the cooperative binding of Ca^{2+} to four Ca^{2+} binding sites. While CaM binds Ca^{2+} in the range of 0.1−10 μM (*22*, *80*), several mutational efforts have been made to increase this range, but such attempts often resulted in multiple signal responses with a tradeoff in dynamic range and required stringent calibration (*31*). Clearly, then, the development of Ca^{2+} sensors that are not based on endogenous Ca^{2+} binding proteins would be highly advantageous.

All cells and their subcellular compartments have mechanisms for regulating their pH at a steady-state level. For example, the cytoplasm has a fairly uniform pH range of 7.1−7.3, equivalent to the pH in the ER. An elegant study conducted by Kim and his colleagues reported that the pH in the endoplasmic reticulum of HeLa cells is maintained at 7.07 ± 0.02 (mean ± standard error) at rest and during calcium release (*81*). Using noninvasive measurements, fluorescence ratio imaging, and two independent calibration procedures, they clearly demonstrate that both K^+ and H^+ activities within the ER are similar to that of the cytosol using nigericin and 140 mM K^+. Cells stimulated with either ATP, histamine, or lysophosphatidic acid exhibited increases in cytosolic Ca^{2+} concentration by releasing Ca^{2+} from the ER store. In contrast, parallel measurements indicated that the pH_{ER} remained stable throughout the period of Ca^{2+} release. These findings strongly support the assumption that our probe can be used to measure the rate of release of Ca^{2+} from the ER without interference from a significant change in the pH of the ER in response to cell stimulation.

A problem that plagues nearly all types of Ca^{2+} sensors and probes, including the ones described here, is that of pH sensitivity. This is largely due to the fact that ligand atoms for Ca^{2+} binding are highly charged. Many GFP-based Ca^{2+} sensors (*33*, *66*, *82*) have been utilized to monitor Ca^{2+} signals in vivo, although their pK_as are also near physiological pH like that of our sensor developed here. The pH sensitivity of GFP variants presents a challenge for the development of GFP-based biosensors. The development of yellow fluorescent protein (YFP) variants is an example of efforts to improve pH resistance. The first generation of YFP, EYFP (GFP-Ser65Gly/Ser72Ala/Thr203Tyr), includes a tyrosine residue substituted at position Thr203 (T203Y). The $\pi-\pi$ interaction between Tyr203 and the chromophore phenol ring results in a red shift in both the excitation and emission wavelengths, resulting in a yellow fluorescent variant of GFP. The mutations in EYFP, however, resulted in a variant more pH sensitive (pK_a = 6.9) than that of GFP (*79*, *83*). A second-generation EYFP (EYFP-Val68Leu/Gln69Lys) slightly improved its acid resistance with a pK_a of ∼6.4 (*79*). Additionally, third-generation derivatives, Citrine (EYFP-Val68Leu/Gln69Met; pK_a = 5.7) (*84*) and Verus (EYFP-Phe46Leu/Phe64Lue/Met153Thr/Val163Ala/Ser175Gly; pK_a = 6.0) (*85*), have a high pH resistance. Another example of a GFP variant with high pH resistance is cyan-green fluorescent protein (CGFP). The T203Y mutation in enhanced cyan fluorescent protein results in a decrease in pK_a from ∼ 6 to <4.0 (*86*). Thus, it should be possible to improve the pH sensitivity of our Ca^{2+} sensors through specific mutations in the future.

Our strategy for developing Ca^{2+} sensors by grafting only the Ca^{2+}-binding motif into a sensitive location of EGFP represents a new approach with several advantages. First,

without using natural Ca^{2+} binding proteins such as CaM and TnC and their numerous target proteins such as M13, kinases, etc., our approach eliminates interference due to competition with endogenous CaM and TnC and their target receptor proteins. To the best of our knowledge, this is the first description of a GFP-based Ca^{2+} sensor that uses neither a natural Ca^{2+} binding protein such as CaM or TnC nor one of its numerous target proteins. Second, our sensor permits a fuller range of Ca^{2+} responses to be recorded with minimal perturbation of the cell-intrinsic Ca^{2+} signaling networks. Since the quantum yield of the sensors is comparable to that of EGFP-wt (Table 1), the expression of the sensor at a micromolar concentration is usually sufficient to permit cellular imaging. The Ca^{2+} buffer effect of the sensor is expected to be negligible, since the GFP sensor concentration is relatively low (~1 μM) compared to the Ca^{2+} concentration in the ER (>100 μM). Third, by varying the Ca^{2+}-binding motifs through the addition of flanking EF-hand helices or glycine linkers, this grafting approach yields a specific range of biologically useful Ca^{2+} affinities. Currently available sensors have K_d values that range from ~0.2 μM to 0.5 mM (*31*, *32*, *34*, *35*, *65*, *82*). With a K_d range of 0.4−2.0 mM, our sensors have the lowest affinity reported to date, and their K_d is well matched for measurements of Ca^{2+} concentrations in cellular compartments containing high Ca^{2+} concentrations. Fourth, the newly developed sensors are ratiometric and not FRET-based, which may allow them to be used with a slightly wider range of secondary fluorophores that might otherwise overlap with the CFP excitation or YFP emission spectra of most FRET probes. The dynamic range of Ca-G1-37 is 1.8, which is comparable to the reported value of the YC2.1 series of Ca^{2+} sensors (*31*). Given the unique versatility of our sensor, we envision that it can be further modified in dynamic range and pH sensitivity to be targeted to other cellular compartments in the future. We envision that this approach will provide tools for studying the contribution of the ER and other cellular compartments to cellular Ca^{2+} signaling in a wide variety of cell types, under different physiological conditions, and in various disease states.

ACKNOWLEDGMENT

We thank Dr. Wei Yang, Dan Adams, and Michael Kirberger for their critical review of the manuscript and helpful discussions, Dr. Liana Artinian and Birgit Neuhaus for assistance with confocal and conventional imaging, Dr. Zhi-ren Liu and Christie Carter for the help with cell culture techniques and suggestions, and Dr. Beth Finch and the members of the Yang research group for their helpful discussions.

SUPPORTING INFORMATION AVAILABLE

CD structural analysis of Ca^{2+} sensor constructs and pH sensitivity of Ca^{2+} sensor constructs. This material is available free of charge via the Internet at http://pubs.acs.org.

REFERENCES

1. Berridge, M. J., Bootman, M. D., and Lipp, P. (1998) Calcium: A life and death signal, *Nature 395*, 645−648.
2. Burdakov, D., Petersen, O. H., and Verkhratsky, A. (2005) Intraluminal calcium as a primary regulator of endoplasmic reticulum function, *Cell Calcium 38*, 303−310.
3. Parekh, A. B., and Putney, J. W., Jr. (2005) Store-operated calcium channels, *Physiol. Rev. 85*, 757−810.
4. Corbett, E. F., and Michalak, M. (2000) Calcium, a signaling molecule in the endoplasmic reticulum? *Trends Biochem. Sci. 25*, 307−311.
5. Petersen, O. H., Tepikin, A., and Park, M. K. (2001) The endoplasmic reticulum: One continuous or several separate Ca^{2+} stores? *Trends Neurosci. 24*, 271−276.
6. Verkhratsky, A., and Petersen, O. H. (2002) The endoplasmic reticulum as an integrating signalling organelle: From neuronal signalling to neuronal death, *Eur. J. Pharmacol. 447*, 141−154.
7. Rizzuto, R., and Pozzan, T. (2006) Microdomains of intracellular Ca^{2+}: Molecular determinants and functional consequences, *Physiol. Rev. 86*, 369−408.
8. Scorrano, L., Oakes, S. A., Opferman, J. T., Cheng, E. H., Sorcinelli, M. D., Pozzan, T., and Korsmeyer, S. J. (2003) BAX and BAK regulation of endoplasmic reticulum Ca^{2+}: A control point for apoptosis, *Science 300*, 135−139.
9. Scorrano, L. (2003) Divide et impera: Ca^{2+} signals, mitochondrial fission and sensitization to apoptosis, *Cell Death Differ. 10*, 1287−1289.
10. Ermak, G., Morgan, T. E., and Davies, K. J. (2001) Chronic overexpression of the calcineurin inhibitory gene DSCR1 (Adapt78) is associated with Alzheimer's disease, *J. Biol. Chem. 276*, 38787−38794.
11. Lin, X., Sikkink, R. A., Rusnak, F., and Barber, D. L. (1999) Inhibition of calcineurin phosphatase activity by a calcineurin B homologous protein, *J. Biol. Chem. 274*, 36125−36131.
12. Zhang, X., and Joseph, S. K. (2001) Effect of mutation of a calmodulin binding site on Ca^{2+} regulation of inositol trisphosphate receptors, *Biochem. J. 360*, 395−400.
13. Bers, D. M., and Guo, T. (2005) Calcium signaling in cardiac ventricular myocytes, *Ann. N.Y. Acad. Sci. 1047*, 86−98.
14. Nelson, M. R., and Chazin, W. J. (1998) Structures of EF-hand Ca^{2+}-binding proteins: Diversity in the organization, packing and response to Ca^{2+} binding, *BioMetals 11*, 297−318.
15. Wehrens, X. H., Lehnart, S. E., and Marks, A. R. (2005) Intracellular calcium release and cardiac disease, *Annu. Rev. Physiol. 67*, 69−98.
16. Yano, M., Ikeda, Y., and Matsuzaki, M. (2005) Altered intracellular Ca^{2+} handling in heart failure, *J. Clin. Invest. 115*, 556−564.
17. Mattson, M. P., and Chan, S. L. (2003) Neuronal and glial calcium signaling in Alzheimer's disease, *Cell Calcium 34*, 385−397.
18. Takahashi, A., Camacho, P., Lechleiter, J. D., and Herman, B. (1999) Measurement of intracellular calcium, *Physiol. Rev. 79*, 1089−1125.
19. Katerinopoulos, H. E., and Foukaraki, E. (2002) Polycarboxylate fluorescent indicators as ion concentration probes in biological systems, *Curr. Med. Chem. 9*, 275−306.
20. Chiesa, A., Rapizzi, E., Tosello, V., Pinton, P., de Virgilio, M., Fogarty, K. E., and Rizzuto, R. (2001) Recombinant aequorin and green fluorescent protein as valuable tools in the study of cell signalling, *Biochem. J. 355*, 1−12.
21. Zhang, J., Campbell, R. E., Ting, A. Y., and Tsien, R. Y. (2002) Creating new fluorescent probes for cell biology, *Nat. Rev. Mol. Cell Biol. 3*, 906−918.
22. Demaurex, N. (2005) Calcium measurements in organelles with Ca^{2+}-sensitive fluorescent proteins, *Cell Calcium 38*, 213−222.
23. Solovyova, N., and Verkhratsky, A. (2002) Monitoring of free calcium in the neuronal endoplasmic reticulum: An overview of modern approaches, *J. Neurosci. Methods 122*, 1−12.
24. Giepmans, B. N., Adams, S. R., Ellisman, M. H., and Tsien, R. Y. (2006) The fluorescent toolbox for assessing protein location and function, *Science 312*, 217−224.
25. Steenbergen, J. M., and Fay, F. S. (1996) The quantal nature of calcium release to caffeine in single smooth muscle cells results from activation of the sarcoplasmic reticulum Ca^{2+}-ATPase, *J. Biol. Chem. 271*, 1821−1824.
26. Hofer, A. M., Curci, S., Machen, T. E., and Schulz, I. (1996) ATP regulates calcium leak from agonist-sensitive internal calcium stores, *FASEB J. 10*, 302−308.
27. Hofer, A. M., Schlue, W. R., Curci, S., and Machen, T. E. (1995) Spatial distribution and quantitation of free luminal [Ca] within the InsP3-sensitive internal store of individual BHK-21 cells: Ion dependence of InsP3-induced Ca release and reloading, *FASEB J. 9*, 788−798.
28. Montero, M., Brini, M., Marsault, R., Alvarez, J., Sitia, R., Pozzan, T., and Rizzuto, R. (1995) Monitoring dynamic changes in free

Ca^{2+} concentration in the endoplasmic reticulum of intact cells, *EMBO J. 14*, 5467−5475.
29. Persechini, A., Lynch, J. A., and Romoser, V. A. (1997) Novel fluorescent indicator proteins for monitoring free intracellular Ca^{2+}, *Cell Calcium 22*, 209−216.
30. Romoser, V. A., Hinkle, P. M., and Persechini, A. (1997) Detection in living cells of Ca^{2+}-dependent changes in the fluorescence emission of an indicator composed of two green fluorescent protein variants linked by a calmodulin-binding sequence. A new class of fluorescent indicators, *J. Biol. Chem. 272*, 13270−13274.
31. Miyawaki, A., Llopis, J., Heim, R., McCaffery, J. M., Adams, J. A., Ikura, M., and Tsien, R. Y. (1997) Fluorescent indicators for Ca^{2+} based on green fluorescent proteins and calmodulin, *Nature 388*, 882−887.
32. Palmer, A. E., Jin, C., Reed, J. C., and Tsien, R. Y. (2004) Bcl-2-mediated alterations in endoplasmic reticulum Ca^{2+} analyzed with an improved genetically encoded fluorescent sensor, *Proc. Natl. Acad. Sci. U.S.A. 101*, 17404−17409.
33. Baird, G. S., Zacharias, D. A., and Tsien, R. Y. (1999) Circular permutation and receptor insertion within green fluorescent proteins, *Proc. Natl. Acad. Sci. U.S.A. 96*, 11241−11246.
34. Palmer, A. E., Giacomello, M., Kortemme, T., Hires, S. A., Lev-Ram, V., Baker, D., and Tsien, R. Y. (2006) Ca^{2+} indicators based on computationally redesigned calmodulin-peptide pairs, *Chem. Biol. 13*, 521−530.
35. Nagai, T., Yamada, S., Tominaga, T., Ichikawa, M., and Miyawaki, A. (2004) Expanded dynamic range of fluorescent indicators for Ca^{2+} by circularly permuted yellow fluorescent proteins, *Proc. Natl. Acad. Sci. U.S.A. 101*, 10554−10559.
36. Heim, N., and Griesbeck, O. (2004) Genetically encoded indicators of cellular calcium dynamics based on troponin C and green fluorescent protein, *J. Biol. Chem. 279*, 14280−14286.
37. Mank, M., Reiff, D. F., Heim, N., Friedrich, M. W., Borst, A., and Griesbeck, O. (2006) A FRET-based calcium biosensor with fast signal kinetics and high fluorescence change, *Biophys. J. 90*, 1790−1796.
38. Evanko, D. S., and Haydon, P. G. (2005) Elimination of environmental sensitivity in a cameleon FRET-based calcium sensor via replacement of the acceptor with Venus, *Cell Calcium 37*, 341−348.
39. Zou, J., Ye, Y., Welshhans, K., Lurtz, M., Ellis, A. L., Louis, C., Rehder, V., and Yang, J. J. (2005) Expression and optical properties of green fluorescent protein expressed in different cellular environments, *J. Biotechnol. 119*, 368−378.
40. Kozak, M. (1989) The scanning model for translation: An update, *J. Cell Biol. 108*, 229−241.
41. Crameri, A., Whitehorn, E. A., Tate, E., and Stemmer, W. P. (1996) Improved green fluorescent protein by molecular evolution using DNA shuffling, *Nat. Biotechnol. 14*, 315−319.
42. Fukuda, H., Arai, M., and Kuwajima, K. (2000) Folding of green fluorescent protein and the cycle3 mutant, *Biochemistry 39*, 12025−12032.
43. Minta, A., Kao, J. P., and Tsien, R. Y. (1989) Fluorescent indicators for cytosolic calcium based on rhodamine and fluorescein chromophores, *J. Biol. Chem. 264*, 8171−8178.
44. Gampp, H., Maeder, M., Meyer, C. J., and Zuberbuhler, A. D. (1986) Calculation of equilibrium constants from multiwavelength spectroscopic data. IV: Model-free least-squares refinement by use of evolving factor analysis, *Talanta 33*, 943−951.
45. Fan, F., and Gadda, G. (2005) On the catalytic mechanism of choline oxidase, *J. Am. Chem. Soc. 127*, 2067−2074.
46. Caroppo, R., Colella, M., Colasuonno, A., DeLuisi, A., Debellis, L., Curci, S., and Hofer, A. M. (2003) A reassessment of the effects of luminal [Ca^{2+}] on inositol 1,4,5-trisphosphate-induced Ca^{2+} release from internal stores, *J. Biol. Chem. 278*, 39503−39508.
47. Ye, Y., Lee, H. W., Yang, W., Shealy, S., and Yang, J. J. (2005) Probing site-specific calmodulin calcium and lanthanide affinity by grafting, *J. Am. Chem. Soc. 127*, 3743−3750.
48. Ye, Y., Lee, H. W., Yang, W., and Yang, J. J. (2005) Calcium and lanthanide affinity of the EF-loops from the C-terminal domain of calmodulin, *J. Inorg. Biochem. 99*, 1376−1383.
49. Tsien, R. Y. (1998) The green fluorescent protein, *Annu. Rev. Biochem. 67*, 509−544.
50. Finney, L. A., and O'Halloran, T. V. (2003) Transition metal speciation in the cell: Insights from the chemistry of metal ion receptors, *Science 300*, 931−936.
51. Rae, T. D., Schmidt, P. J., Pufahl, R. A., Culotta, V. C., and O'Halloran, T. V. (1999) Undetectable intracellular free copper: The requirement of a copper chaperone for superoxide dismutase, *Science 284*, 805−808.
52. Pelham, H. R. (1996) The dynamic organisation of the secretory pathway, *Cell Struct. Funct. 21*, 413−419.
53. Hofer, A. M., Landolfi, B., Debellis, L., Pozzan, T., and Curci, S. (1998) Free [Ca^{2+}] dynamics measured in agonist-sensitive stores of single living intact cells: A new look at the refilling process, *EMBO J. 17*, 1986−1995.
54. Ye, Y., Lee, H. W., Yang, W., Shealy, S. J., Wilkins, A. L., Liu, Z. R., Torshin, I., Harrison, R., Wohlhueter, R., and Yang, J. J. (2001) Metal binding affinity and structural properties of an isolated EF-loop in a scaffold protein, *Protein Eng. 14*, 1001−1013.
55. Ye, Y., Shealy, S., Lee, H. W., Torshin, I., Harrison, R., and Yang, J. J. (2003) A grafting approach to obtain site-specific metal-binding properties of EF-hand proteins, *Protein Eng. 16*, 429−434.
56. Michalak, M., Corbett, E. F., Mesaeli, N., Nakamura, K., and Opas, M. (1999) Calreticulin: One protein, one gene, many functions, *Biochem. J. 344* (Part 2), 281−292.
57. Topell, S., Hennecke, J., and Glockshuber, R. (1999) Circularly permuted variants of the green fluorescent protein, *FEBS Lett. 457*, 283−289.
58. Chiang, C. F., Okou, D. T., Griffin, T. B., Verret, C. R., and Williams, M. N. (2001) Green fluorescent protein rendered susceptible to proteolysis: Positions for protease-sensitive insertions, *Arch. Biochem. Biophys. 394*, 229−235.
59. Abedi, M. R., Caponigro, G., and Kamb, A. (1998) Green fluorescent protein as a scaffold for intracellular presentation of peptides, *Nucleic Acids Res. 26*, 623−630.
60. Doi, N., and Yanagawa, H. (1999) Design of generic biosensors based on green fluorescent proteins with allosteric sites by directed evolution, *FEBS Lett. 453*, 305−307.
61. Churchill, G. C., and Louis, C. F. (1999) Imaging of intracellular calcium stores in single permeabilized lens cells, *Am. J. Physiol. 276*, C426−C434.
62. Park, M. K., Petersen, O. H., and Tepikin, A. V. (2000) The endoplasmic reticulum as one continuous Ca^{2+} pool: Visualization of rapid Ca^{2+} movements and equilibration, *EMBO J. 19*, 5729−5739.
63. Shmigol, A. V., Eisner, D. A., and Wray, S. (2001) Simultaneous measurements of changes in sarcoplasmic reticulum and cytosolic, *J. Physiol. 531*, 707−713.
64. Robert, V., De Giorgi, F., Massimino, M. L., Cantini, M., and Pozzan, T. (1998) Direct monitoring of the calcium concentration in the sarcoplasmic and endoplasmic reticulum of skeletal muscle myotubes, *J. Biol. Chem. 273*, 30372−30378.
65. Truong, K., Sawano, A., Mizuno, H., Hama, H., Tong, K. I., Mal, T. K., Miyawaki, A., and Ikura, M. (2001) FRET-based in vivo Ca^{2+} imaging by a new calmodulin-GFP fusion molecule, *Nat. Struct. Biol. 8*, 1069−1073.
66. Nakai, J., Ohkura, M., and Imoto, K. (2001) A high signal-to-noise Ca^{2+} probe composed of a single green fluorescent protein, *Nat. Biotechnol. 19*, 137−141.
67. Black, D. J., Tran, Q. K., and Persechini, A. (2004) Monitoring the total available calmodulin concentration in intact cells over the physiological range in free Ca^{2+}, *Cell Calcium 35*, 415−425.
68. Mori, M. X., Erickson, M. G., and Yue, D. T. (2004) Functional stoichiometry and local enrichment of calmodulin interacting with Ca^{2+} channels, *Science 304*, 432−435.
69. Yang, J. J. (2006) Calmodulin, the Surprises Continue, *Calcium Binding Proteins 1*, 65−66.
70. Trudeau, M. C., and Zagotta, W. N. (2003) Calcium/calmodulin modulation of olfactory and rod cyclic nucleotide-gated ion channels, *J. Biol. Chem. 278*, 18705−18708.
71. Peracchia, C. (2004) Chemical gating of gap junction channels: Roles of calcium, pH and calmodulin, *Biochim. Biophys. Acta 1662*, 61−80.
72. Persechini, A. (2002) Monitoring the intracellular free Ca^{2+}-calmodulin concentration with genetically-encoded fluorescent indicator proteins, *Methods Mol. Biol. 173*, 365−382.
73. Maier, L. S., Ziolo, M. T., Bossuyt, J., Persechini, A., Mestril, R., and Bers, D. M. (2006) Dynamic changes in free Ca-calmodulin levels in adult cardiac myocytes, *J. Mol. Cell. Cardiol. 41*, 451−458.
74. Jurado, L. A., Chockalingam, P. S., and Jarrett, H. W. (1999) Apocalmodulin, *Physiol. Rev. 79*, 661−682.
75. Saimi, Y., and Kung, C. (2002) Calmodulin as an ion channel subunit, *Annu. Rev. Physiol. 64*, 289−311.

76. Hasan, M. T., Friedrich, R. W., Euler, T., Larkum, M. E., Giese, G., Both, M., Duebel, J., Waters, J., Bujard, H., Griesbeck, O., Tsien, R. Y., Nagai, T., Miyawaki, A., and Denk, W. (2004) Functional fluorescent Ca^{2+} indicator proteins in transgenic mice under TET control, *PLoS Biol. 2*, 763−775.
77. Reiff, D. F., Thiel, P. R., and Schuster, C. M. (2002) Differential regulation of active zone density during long-term strengthening of *Drosophila* neuromuscular junctions, *J. Neurosci. 22*, 9399−9409.
78. Fiala, A., Spall, T., Diegelmann, S., Eisermann, B., Sachse, S., Devaud, J. M., Buchner, E., and Galizia, C. G. (2002) Genetically expressed cameleon in *Drosophila melanogaster* is used to visualize olfactory information in projection neurons, *Curr. Biol. 12*, 1877−1884.
79. Miyawaki, A., Griesbeck, O., Heim, R., and Tsien, R. Y. (1999) Dynamic and quantitative Ca^{2+} measurements using improved cameleons, *Proc. Natl. Acad. Sci. U.S.A. 96*, 2135−2140.
80. Tsien, R. Y. (2005) Building and breeding molecules to spy on cells and tumors, *FEBS Lett. 579*, 927−932.
81. Kim, J. H., Johannes, L., Goud, B., Antony, C., Lingwood, C. A., Daneman, R., and Grinstein, S. (1998) Noninvasive measurement of the pH of the endoplasmic reticulum at rest and during calcium release, *Proc. Natl. Acad. Sci. U.S.A. 95*, 2997−3002.
82. Nagai, T., Sawano, A., Park, E. S., and Miyawaki, A. (2001) Circularly permuted green fluorescent proteins engineered to sense Ca^{2+}, *Proc. Natl. Acad. Sci. U.S.A. 98*, 3197−3202.
83. Ormo, M., Cubitt, A. B., Kallio, K., Gross, L. A., Tsien, R. Y., and Remington, S. J. (1996) Crystal structure of the *Aequorea victoria* green fluorescent protein, *Science 273*, 1392−1395.
84. Griesbeck, O., Baird, G. S., Campbell, R. E., Zacharias, D. A., and Tsien, R. Y. (2001) Reducing the environmental sensitivity of yellow fluorescent protein. Mechanism and applications, *J. Biol. Chem. 276*, 29188−29194.
85. Nagai, T., Ibata, K., Park, E. S., Kubota, M., Mikoshiba, K., and Miyawaki, A. (2002) A variant of yellow fluorescent protein with fast and efficient maturation for cell-biological applications, *Nat. Biotechnol. 20*, 87−90.
86. Sawano, A., and Miyawaki, A. (2000) Directed evolution of green fluorescent protein by a new versatile PCR strategy for site-directed and semi-random mutagenesis, *Nucleic Acids Res. 28*, E78.

BI7007307